13th International Symposium on Turbulence and Shear Flow Phenomena (TSFP13)
Montreal, Canada, June 25–28, 2024

HIGH-ORDER MOMENT SCALING OF NEAR-WALL TURBULENCE FOR ARBITRARY VELOCITIES: AN EXTENDED SYMMETRY APPROACH

Simon Görtz[1,2], Martin Oberlack[1,2] and Jonathan Laux[1]
[1]Technical University of Darmstadt, Chair of Fluid Dynamics,
Otto-Berndt-Straße 2, 64287 Darmstadt, Germany
[2]TU Darmstadt, Centre for Computational Engineering,
Dolivostrasse 15, 64293 Darmstadt, Germany

Sergio Hoyas
Instituto Universitario de Matemática Pura y Aplicada, Universitat Politècnica de València,
Camino de Vera, 46024 València, Spain

ABSTRACT

Presently, we derive and validate scaling laws for arbitrary turbulent one-point velocity moments in wall-bounded flows, focusing on moments from spanwise and wall-normal velocity components. The scaling laws are derived using a symmetry analysis of the underlying set of Navier-Stokes equations from which the infinite moment hierarchy is derived and are therefore first principle-based. They are subsequently validated using new DNS data, revealing a hidden Reynolds number dependency and the fact that scaling is determined by the lowest order moment. Consistency with DNS data confirms the validity of the scaling laws even for sensitive fluctuating moments.

DERIVATION OF SCALING LAWS

The subsequent analysis is based on the Navier-Stokes equations,

$$\frac{\partial U_i}{\partial t}+U_k\frac{\partial U_i}{\partial x_k}+\frac{\partial P}{\partial x_i}-\nu\frac{\partial^2 U_i}{\partial x_k\partial x_k}=0\,,\quad \frac{\partial U_k}{\partial x_k}=0, \tag{1}$$

where $t\in\mathbb{R}^+$, $\boldsymbol{x}\in\mathbb{R}^3$, $\boldsymbol{U}=\boldsymbol{U}(\boldsymbol{x},t)$, $P=P(\boldsymbol{x},t)$, and ν represent time, position vector, instantaneous velocity vector, pressure, and kinematic viscosity, respectively. In contrast to Reynolds' decomposition, i.e. $U_k=\bar{U}_k+u_k$, where $\overline{(\cdot)}$ and u_k are respectively mean and fluctuation quantities, we consider statistical moments based on the instantaneous flow quantities. Consequently, the generic multipoint velocity moments in multi index notation are defined by

$$H_{i_{\{n\}}}=H_{i_{(1)}\dots i_{(n)}}=\overline{U_{i_{(1)}}(\boldsymbol{x}_{(1)},t)\cdot\ldots\cdot U_{i_{(n)}}(\boldsymbol{x}_{(n)},t)}\,. \tag{2}$$

With that definition and analogous to Oberlack *et al.* (2022), the multipoint moment equation (MPME) for the velocity yields

$$\frac{\partial H_{i_{\{n\}}}}{\partial t}+\sum_{l=1}^{n}\left[\frac{\partial H_{i_{\{n+1\}}[i_{(n)}\mapsto k_{(l)}]}[\boldsymbol{x}_{(n)}\mapsto\boldsymbol{x}_{(l)}]}{\partial x_{k_{(l)}}}+\frac{\partial I_{i_{\{n-1\}}[l]}}{\partial x_{i_{(l)}}}-\nu\frac{\partial^2 H_{i_{\{n\}}}}{\partial x_{k_{(l)}}\partial x_{k_{(l)}}}\right]=0. \tag{3}$$

The moment $I_{i_{\{n-1\}}[l]}$ refers to the pressure-velocity correlation and correlates the pressure at l-th. point with $n-1$ velocities (see Oberlack & Rosteck, 2010; Oberlack *et al.*, 2015).

In the following, we carry out a symmetry analysis, based on the Navier-Stokes equation (1) and the infinite dimensional system (3). Details on the symmetry theory for generic multipoint moments are presented in depth in the planned publication by Görtz & Oberlack (2024). In the current work we aim to compare the theory with new DNS data, why we restrict the consideration to on one-point statistics, i.e. $\boldsymbol{x}=\boldsymbol{x}_{(1)}=\boldsymbol{x}_{(2)}=\ldots=\boldsymbol{x}_{(n)}$. The corresponding one-point moments are accordingly denoted by $H^{(0)}_{i_{\{n\}}}$. As the theory was successfully presented in Oberlack *et al.* (2022) and validated in Hoyas *et al.* (2022) for mean velocity moments composed of U_1, we focus in the current work on the n^{th} moments of U_2 and U_3, i.e. $\overline{U_{[i]}}$, where the square bracket indicates that no summation is applied.

Very briefly, let us introduce the idea of a form-invariant Lie symmetry transformation $\boldsymbol{x}^*=\boldsymbol{\phi}(\boldsymbol{x},\boldsymbol{y};a)$, $\boldsymbol{y}^*=\boldsymbol{\psi}(\boldsymbol{x},\boldsymbol{y};a)$, leaving a differential equation $\boldsymbol{F}=0$ unchanged. Globally, this means that

$$\begin{aligned}&\boldsymbol{F}\left(\boldsymbol{x},\boldsymbol{y},\boldsymbol{y}^{(1)},\boldsymbol{y}^{(2)},\ldots,\boldsymbol{y}^{(p)}\right)=0\\ \Leftrightarrow\quad &\boldsymbol{F}\left(\boldsymbol{x}^*,\boldsymbol{y}^*,\boldsymbol{y}^{*(1)},\boldsymbol{y}^{*(2)},\ldots,\boldsymbol{y}^{*(p)}\right)=0,\end{aligned} \tag{4}$$

with the p^{th} derivatives of $\boldsymbol{y}$ is defined as $\boldsymbol{y}^{(p)}$.

The symmetry transformations of the system (3) known so far are divided into (i) those inherited from

the Navier-Stokes equations (1) to (3) and (ii) those based on the statistical treatment which are found only in (3) and are therefore called statistical symmetries.

Of the nine symmetries of the inviscid Navier-Stokes equations (1), i.e. the Euler equations, the combined space-time scaling symmetry, including scaling of pressure and velocity, transforms for in the moment frame to

$$\begin{aligned}\bar{T}_{Sx/St}:\ t^* &= \mathrm{e}^{a_{St}}t,\ \ \boldsymbol{x}^*_{(i)} = \mathrm{e}^{a_{Sx}}\boldsymbol{x}_{(i)},\\ \bar{\boldsymbol{U}}^* &= \mathrm{e}^{a_{Sx}-a_{St}}\bar{\boldsymbol{U}}^*, \mathbf{H}^*_{\{n\}} = \mathrm{e}^{n(a_{Sx}-a_{St})}\mathbf{H}_{\{n\}}.\end{aligned} \tag{5}$$

The translation symmetry of space is simply preserved in the moment frame,

$$\bar{T}_{x_i}: t^* = t, \boldsymbol{x}^*_{(i)} = \boldsymbol{x}_{(i)} + \boldsymbol{a}_{\boldsymbol{x}}, \bar{\boldsymbol{U}}^* = \bar{\boldsymbol{U}}^*, \mathbf{H}^*_{\{n\}} = \mathbf{H}_{\{n\}}. \tag{6}$$

The proof of form invariance is easily obtained by substituting (5) and (6) into (3).

As mentioned before, different scalings in space and time require vanishing of the viscous term. Therefore, caution is required at this point, because in principle, the Navier-Stokes equation (1) admits only one scaling symmetry. Only the Euler equations admit the two scaling symmetries (5). A detailed explanation why preservation of both scaling symmetries and consideration of the asymptotic limit $\nu \to 0^+$ is reasonable for the construction of scaling laws is presented in Görtz & Oberlack (2024). There, we carry out a boundary layer-like singular asymptotics in distance space $\boldsymbol{r}_{(i)} = \boldsymbol{x}_{(i)} - \boldsymbol{x}_{(0)}$. The small expansion parameter is the Kolmogorov length scale η determining the small scales where viscosity and dissipation act. This expansion was first derived in Oberlack & Peters (1993) for isotropic turbulence and the two-point moment equation. Subsequently, the MPME decompose into two equations. The large scales, much larger than η, are simply determined by equation (3) with $\nu = 0$. Therefore, scaling laws for moments even of high order are based on this equation why it is, together with its special scaling symmetry (5), the basis for the subsequent analyses. The second equation stemming from the asymptotic analysis is similar to the classical boundary layer equation. It acts on small scales on the order of η where viscosity and dissipation are dominant.

As mentioned above, the statistical symmetries play a central role in the derivation of scaling laws. They were first derived in Oberlack & Rosteck (2010) and in Wacławczyk *et al.* (2014) their physical meaning were pointed out. The translation symmetry in the moments

$$\begin{aligned}\bar{T}'_{\{n\}}:\ t^* &= t,\ \ \boldsymbol{x}^*_{(i)} = \boldsymbol{x}_{(i)},\\ \bar{\boldsymbol{U}}^* &= \bar{\boldsymbol{U}} + \boldsymbol{a},\ \ \mathbf{H}^*_{\{n\}} = \mathbf{H}_{\{n\}} + \mathbf{a}^H_{\{n\}}\end{aligned} \tag{7}$$

conforms to non-gaussianity. The statistical scaling symmetry in the moments only

$$\begin{aligned}\bar{T}'_s:\ t^* &= t,\ \ \boldsymbol{x}^*_{(i)} = \boldsymbol{x}_{(i)},\\ \bar{\boldsymbol{U}}^* &= \mathrm{e}^{a_{Ss}}\bar{\boldsymbol{U}},\ \ \mathbf{H}^*_{\{n\}} = \mathrm{e}^{a_{Ss}}\mathbf{H}_{\{n\}},\end{aligned} \tag{8}$$

can be traced back to intermittency. It stems from the linearity of the infinite system (3).

Finally for the consideration of plane shear flows as it is done in this work, the MPME (3) admits additional symmetries. With x_2 the wall-normal coordinate it allows translation of moments with a linear term in x_2,

$$\begin{aligned}\bar{T}'_L:\ t^* &= t,\ \ \boldsymbol{x}^*_{(i)} = \boldsymbol{x}_{(i)},\\ \bar{\boldsymbol{U}}^* &= \bar{\boldsymbol{U}},\ \ \mathbf{H}^*_{\{n\}} = \mathbf{H}_{\{n\}} + x_2\mathbf{a}^L_{\{n\}},\end{aligned} \tag{9}$$

This symmetry has already been discovered in Rosteck (2014) and is further specified in Görtz & Oberlack (2024). As we will see later, it leads to a linear correction of the scaling laws in the log region of the channel flow. For the core region, this symmetry is broken as it is inconsistent with the requirement of scaling symmetric to the center of the channel. We see later that the prefactor of the linear term is very small for both the U_2 and U_3 moments in the logarithmic region, but by no means negligible.

With this, invariant solutions for $\overline{U^n_{[i]}}$ for $i = 2,3$ and $n \geq 2$ are derived from the discussed symmetries, rather similar to $\overline{U^n_1}$ in Oberlack *et al.* (2022). Also in this work, we restrict ourselves to one-point statistics in comparison with the DNS data. One point moments arise as special case of the complete set of invariant solution for arbitrary multi-point moments $\mathbf{H}_{\{n\}}$ derived in Görtz & Oberlack (2024). There, also the symmetry reduction of the MPME (3) is proven. We combine the groups (5), (7), (8) and (9), which gives us the global form of the transformation,

$$\begin{aligned}\bar{T}:\ x_2^* &= \mathrm{e}^{a_{Sx}}x_2,\ \ \overline{U_1}^* = \mathrm{e}^{a_{Sx}-a_{St}+a_{Ss}}\overline{U_1},, \\ \overline{U^2_{[i]}}^* &= \mathrm{e}^{2(a_{Sx}-a_{St})+a_{Ss}}\overline{U^2_{[i]}} + x_2a^L_{[i]_{\{2\}}} + a^H_{[i]_{\{2\}}}, \dots, \\ \overline{U^n_{[i]}}^* &= \mathrm{e}^{n(a_{Sx}-a_{St})+a_{Ss}}\overline{U^n_{[i]}} + x_2a^L_{[i]_{\{n\}}} + a^H_{[i]_{\{n\}}}\end{aligned} \tag{10}$$

Here, a_{Sx}, a_{St}, and a_{Ss} are the parameters of the combined three-parameter scaling group. The first moment of $i = 2,3$ does not appear, since there is no mean flow in these directions. The characteristic system, describing invariant solutions of the spanwise and wall-normal velocity moments, reads

$$\begin{aligned}&\frac{\mathrm{d}x_2}{a_{Sx}x_2 + a_{x_2}} = \frac{\mathrm{d}\overline{U_1}}{[a_{Sx} - a_{St} + a_{Ss}]\overline{U_1} + a^H_{[1]_{\{1\}}}} = \dots\\ &\frac{\mathrm{d}\overline{U^2_{[i]}}}{[2(a_{Sx} - a_{St}) + a_{Ss}]\overline{U^2_{[i]}} + a^H_{[i]_{\{2\}}} + x_2a^L_{[i]_{\{2\}}}} = \dots\\ &= \frac{\mathrm{d}\overline{U^n_{[i]}}}{[n(a_{Sx} - a_{St}) + a_{Ss}]\overline{U^n_{[i]}} + a^H_{[i]_{\{n\}}} + x_2a^L_{[i]_{\{n\}}}}.\end{aligned} \tag{11}$$

For details on deriving the characteristic system from the global form of transformations, we refer to Görtz & Oberlack (2024).

In the context of integrating (11), we need to distinguish two cases, i.e. the solutions corresponding to

the logarithmic and the center region of the channel flow (see Oberlack *et al.*, 2022). Depending on where scaling laws are considered, different parameters turn out to be symmetry breaking, i.e. restricting the group parameters. The pivotal parameter governing the logarithmic wall-near region is the wall shear stress velocity $u_\tau = \sqrt{\tau_w/\rho}$, where τ_w is the wall shear stress, and ρ represents density. u_τ subsequently forms the exclusive near-wall velocity scale. Consequently, for a prescribed specific value, adherence to the scaling of the mean velocity as dictated by Eq.(10), the wall shear stress velocity leads to the symmetry-breaking and, hence, $a_{Sx} - a_{St} + a_{Ss} = 0$. Consequently, the integration of Eq.(11) under this restriction leads to a reduced parameter dependence for the scaling laws in the logarithmic region due to integration of the first two terms in (11), and the higher moments follow from the first and further terms.

$$\overline{U^n_{[i]}} = \tilde{C}_{[i]_{\{n\}}} \left(x_2 + \frac{a_{x_2}}{a_{Sx}} \right)^{\omega(n-1)} + \frac{a^L_{[i]_{\{n\}}}}{a_{Sx}(1+\omega(1-n))} x_2 + \frac{a^H_{[i]_{\{n\}}}(1+\omega(1-n)) - a^L_{[i]_{\{n\}}} \frac{a_{x_2}}{a_{Sx}}}{a_{Sx}\omega(1-n)(1+\omega(1-n))}. \quad (12)$$

Here, $\omega = 1 - a_{St}/a_{Sx}$ is a universal constant, and $\tilde{C}_{n,[i]}$ emerges as constant of integration. Similar to the results in Oberlack *et al.* (2022) for the U_1 moments, we find three key results: (i) moments $n \geq 2$ have a power law behavior, where (ii) all n^{th}-order moments are linked with each other by the exponent ω, (iii) the power law behavior is the same for all three U_i components, which will later clearly be proven by the DNS data,

For the scaling laws in the channel core region, as mentioned above, the symmetry of the flow with respect to the channel center is symmetry breaking, i.e. $\mathbf{a}^L_{\{n\}} = 0$. Subsequently, in eq. (11), the factors $(a_{Sx} - a_{St} + a_{Ss}), \ldots, n(a_{Sx} - a_{St}) + a_{Ss}$ are all non-zero. This again gives us power-laws for all moments n, including the mean flow component of U_1, i.e. the first moment. We further find that we can summarize a_{Sx}, a_{St}, and a_{Ss} as two free parameters, since they only occur as ratios. From the exponents for the first two moments, σ_1 and σ_2, the scaling laws for the channel core region follow as

$$\overline{U^n_{[i]}} = \tilde{C}'_{[i]_{\{n\}}} \left(x_2 + \frac{a_{x_2}}{a_{Sx}} \right)^{n(\sigma_2-\sigma_1)+2\sigma_1-\sigma_2} - \frac{a^H_{[i]_{\{n\}}}}{n(a_{Sx} - a_{St}) + a_{Ss}}, \quad (13)$$

Again, all $\tilde{C}'$ are constants of integration, and the group parameters are summarized as $\sigma_1 = 1 - a_{St}/a_{Sx} + a_{Ss}/a_{Sx}$ and $\sigma_2 = 2(1 - a_{St}/a_{Sx}) + a_{Ss}/a_{Sx}$. As can be seen from the scaling laws, the latter exponents of the first two moments determine the exponent of all power laws for the higher order moments.

COMPARISON WITH DNS DATA

The scaling laws (12) and (13) are in the following validated using new DNS data of a plane turbulent channel flow, with a Reynolds number of $Re_\tau = 10^4$ using the code LISO with a grid of about 80 billion points. For further details on this simulation, the reader is referred to Hoyas *et al.* (2022), where, however, for the current comparison, the length of the DNS was doubled again compared to the aforementioned work. In addition to the validation presented in Oberlack *et al.* (2022), we will in the following validate the scaling laws for moments from velocity components $i = 2, 3$. These are of special interest since no mean flow in this direction exists. Therefore, in this case instantaneous moments are identical with the fluctuating moments. In other words, the scaling laws derived in the previous section hold for fluctuating as well as for instantaneous moments.

Validation in the logarithmic region

In the following, the wall normal coordinate in the logarithmic region is denoted by y^+, i.e. $y^+ = 0$ defines the wall. Accordingly, the scaling laws to be validated in the logarithmic region are given by

$$\overline{U^n_{[i]}}^+ = C_{[i]_{\{n\}}} \left(y^+ + A \right)^{\omega(n-1)} + B_{[i]_{\{n\}}} + L_{[i]_{\{n\}}} y^+, \quad \text{for } n \geq 2, \quad (14)$$

where we have summarized the various constant group parameters appearing in eq. (12). For a similar validation of the logarithmic law for the averaged mean velocity, see Hoyas *et al.* (2022) where the von Kármán constant a value was obtained to $\kappa = 0.394$. It is subject of ongoing research whether the data below shows that C_n and B_n result in a simple exponential function in n as already shown for the U_1-moments in Oberlack *et al.* (2022).

Fig. 1a and Fig. 1b show the higher U_2 and U_3-moments for $n = 2, 4, 6$ in the logarithmic layer. Therein, we find a comparison between the DNS data and the fitted theoretical result (12). The power law scaling behavior is clearly visible by the double logarithmic plotting. The universal scaling factor is chosen to $\omega = 0.1$, matching the DNS data and obtaining the best fit for both figures. This again reveals that both moments obey the same scaling behavior.

The two key results of these fits are (i) an extremely good match of the power law with the DNS data for all moments. Their power law scaling is solely determined by the single parameter ω and (ii) the validity of the scaling laws in the log law's range of validity of $y^+ \simeq 400 \ldots 2500$. This range of validity is obtained by considering a power law indicator function analogous to the consideration in Oberlack *et al.* (2022).

Validation in the centre region

In the centre region of the channel, we use the common way to formulate moments in deficit form. This is done by using a shifted coordinate x_2, with origin $x_2 = 0$ on the channel center. First ideas on a symmetry based power law similar to (13) in the centre of a channel flow were formulated in Oberlack (2001). Therein, the mean velocity was derived in deficit form, which is in the current work used for arbitrary moments of U_i with $i = 2, 3$. Therefore, the power law scaling (13) is transformed to the universal deficit form

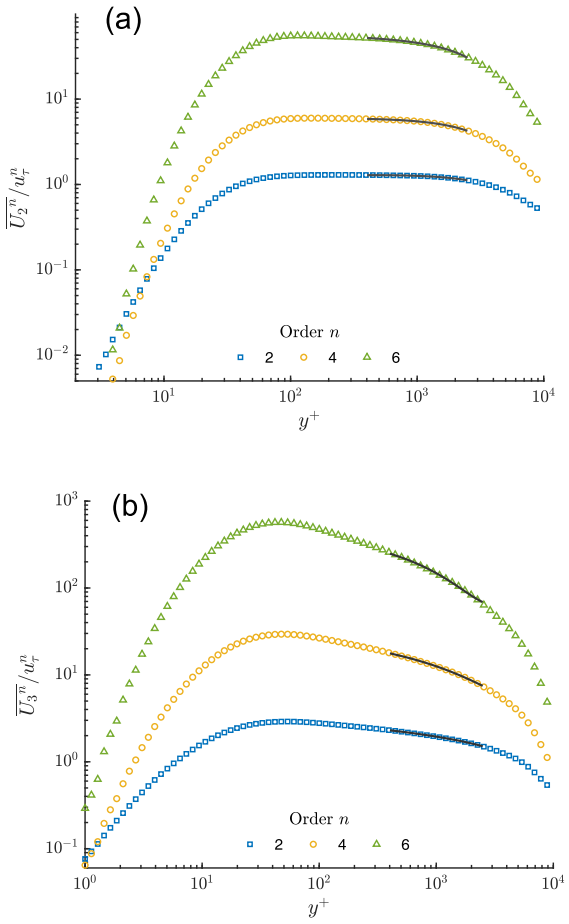

Figure 1: Comparison of moments between theory (solid) and DNS data at $Re_\tau = 10000$ in the range $y^+ \in [400, 2500]$ for U_2 (a) and U_3-moments (b) of order 2, 4, 6 in the logarithmic region. The mentioned y^+ range corresponds to the range of validity of the log-law for the given Reynolds number as shown in Oberlack *et al.* (2022).

$$\frac{\overline{U_i^n}^{(0)} - \overline{U_i^n}}{u_\tau^n} = C'_{i,n} \left(\frac{x_2}{h}\right)^{n(\sigma_2-\sigma_1)+2\sigma_1-\sigma_2} \tag{15}$$

The exponent (0) in $\overline{U_i^n}^{(0)}$ refers to the value of the moment in the centre of the channel at $x_2 = 0$ and, similar to Eq. (14), α' and β' subsume various constants and are presumed to be universal in the core region.

In Fig. 2, we show the moments from the DNS at $Re_\tau = 10^4$ according to the deficit form up to order $n = 6$. It is obvious that for a large range, the moments show identical gradients, independent from the order n. This behavior is, according to the scaling law (15), reachable if $\sigma_1 = \sigma_2$. Consistent with this, the parameters in eq. (15) were fitted, namely to $\sigma_1 = 1.95$ and $\sigma_2 = 1.94$. Indeed, the fit of the core moments here shows a larger relative deviation from the DNS data than for the U_1-moments in Oberlack *et al.* (2022), which might be due to the extremely sensitive fluctuating moments here. However, we argue that against this background eq. (15)

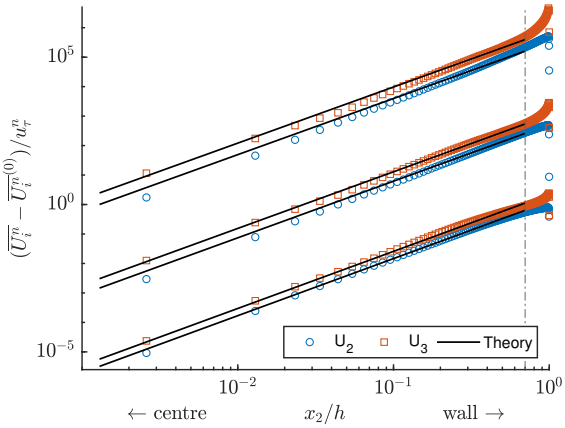

Figure 2: Comparison between theory (solid) and DNS data at $Re_\tau = 10000$ for U_2 and U_3-moments of order 2, 4, 6 (from bottom to top) in the core region.

represents the scaling very well, which is further supported by it being an invariant solution of the moment equations, as we show in Görtz & Oberlack (2024).

Summing up, like the U_1 moments, all U_2 and U_3 moments in the core region scale with a single exponent which is independent of n, i.e. these moments clearly admit strong anomalous scaling. This is accompanied by strongly intermittent *instantaneous* velocities in the channel center, to which we will assign the initially indeterminate velocity scale u^*. Regarding the symmetries in (5) shows that the constant exponent for all velocity moments is accompanied by symmetry breaking

$$a_{Sx} = a_{St}.$$

Thus, the scaling of the instantaneous velocities in (5) is broken by the velocity scale u^* and the scaling of moments by the intermittency symmetry (8) alone is preserved, leading to the observed anomalous scaling. Summing up, scaling of moments in the channel center is fundamentally determined by the statistical symmetries.

Reynolds number dependency

In Görtz & Oberlack (2024) we show how viscosity and Reynolds number affect the scaling laws via deriving an integral constraint for the constants and group parameters in the scaling laws, which subsequently depend on the Reynolds number. This integral constraint includes an integration over the interface between logarithmic region and viscous sublayer. At this surface, values of moments and pressure-velocity correlations are determined by viscous dissipation in the sublayer. This effect is carried through the logarithmic region up into the core region, even though, according to the asymptotic expansion in Görtz & Oberlack (2024), the large structures are mainly determined by inviscid equations. Consequently, in comparison to the logarithmic region, the Reynolds number dependency of the parameters in the deficit law core region is significantly weaker than in the log region, which is right next to the viscous sublayer. For reasons of shortness, the analysis in the current work is restricted to the Reynolds number dependency of the parameters in the logarithmic region.

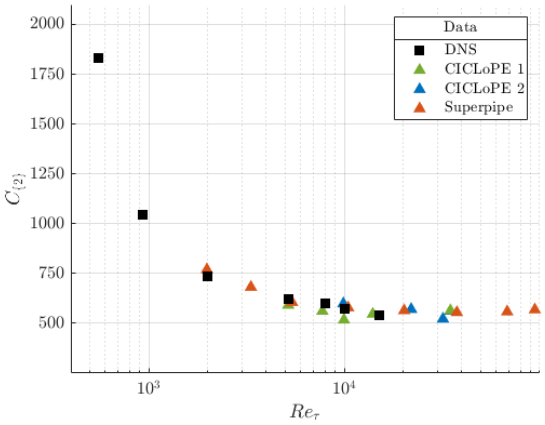

Figure 3: Values for scaling prefactor $C_{[1]_{\{2\}}}$ from eq. (16) fitted for $Re_\tau = 180 \ldots 9.4 \cdot 10^4$

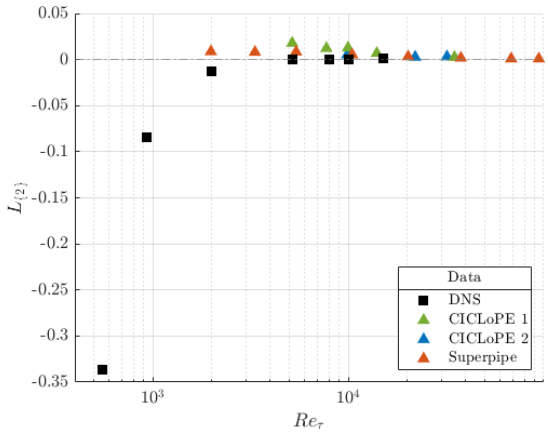

Figure 4: Values for constant $L_{[1]_{\{2\}}}$ from eq. (16), fitted for $Re_\tau = 180 \ldots 9.4 \cdot 10^4$

However, as we aim to compare the coefficients for a broad number of Reynolds numbers, we are restricted to second order U_1 moments, since for these moments a large number of data sets exists. Recall that the scaling law for these moments in the log region is given by

$$\overline{U_1^2}^+ = C_{[1]_{\{2\}}} \left(y^+ + A\right)^\omega + B_{[1]_{\{2\}}} + L_{[1]_{\{2\}}} y^+, \qquad (16)$$

admitting the same power law form as for higher U_2 and U_3 moments as given in (14). It is to point out that the exponent $\omega = 0.1$, determining the power law behavior, is universal and the same for all velocities.
From the statement made above, we assume the Reynolds number dependency to be hidden in C, A, B, L, which are in the following compared for different Reynolds numbers. For the fits of (16), we used DNS data as well as experimental data. The set of experimental data contains data from Hultmark *et al.* (2012) measured at the Princeton Superpipe for $Re_\tau = 2000 \ldots 9.4 \cdot 10^4$ and Zimmerman *et al.* (2019) and Örlü *et al.* (2017) measured at the CICLoPE facility of the University of Bologna for $Re_\tau = 5200 \ldots 3.5 \cdot 10^4$. Fitted parameters referring to experimental data are marked with a triangle ▲. Regarding DNS data, we used data from Hoyas & Jiménez (2006) in a Reynolds number range between $Re_\tau = 180 \ldots 2000$, Lee & Moser (2015) at $Re_\tau = 5200$, Yamamoto & Tsuji (2018) at $Re_\tau = 8000$ and DNS from Hoyas *et al.* (2022) at $Re_\tau = 10^4, 1.5 \cdot 10^4$. Fitted parameters referring to DNS data are marked with a square ■. Note that the fitting range, i.e. the range of y^+ where the constants in the scaling law are fitted, depends on the Reynolds number. This is quite intuitive as the logarithmic region increases with increasing Reynolds number. For the sake of shortness, the fitting range is not displayed here. Figs. 3-6 show the values for the parameters in (16) displayed in semi-logarithmic form over different Reynolds numbers. The first central result, universal for all parameters, is that all data points, regardless of the source of the data, lie consistently on a line, tending to a constant value for high Reynolds numbers. This indicates that from a certainly high Reynolds number, the scaling and therefore the values of the coefficients is truly independent from the Reynolds number. From fig. 4, we further find that the linear term in (16) tends to zero for sufficiently high

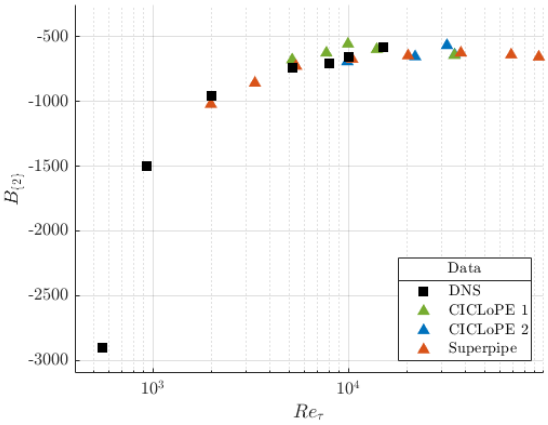

Figure 5: Values for constant $B_{[1]_{\{2\}}}$ from eq. (16), fitted for $Re_\tau = 180 \ldots 9.4 \cdot 10^4$

Reynolds number and is only of notably relevance in the case of lower Reynolds numbers. For the DNS data, the linear term is fitted to zero from a lower Reynolds number than it is for the experimental data. The reason for that might lie in the quality of the measured data but is to be further investigated in future work. It is to note that the offset A, displayed in fig. 6, is universal for all higher moments, independent from their direction and order. This is since A is defined as the ratio between the group parameters a_{x_2}/a_{Sx} and therefore universal for the logarithmic region. In the present work, we have set it to zero throughout due to the sufficiently high Reynolds number.

CONCLUSION

From the above considerations and scaling laws, two main aspects can be concluded. First, for the U_2 and U_3 moments, the exponent of the second order moment is sufficient to obtain the scaling of all higher moments. The scaling is determined in the logarithmic region by ω and for the deficit law by σ_1 respective σ_2. Second, we have shown how the scaling laws are affected by the Reynolds number and how this influence is reduced when moving towards the core region. This has

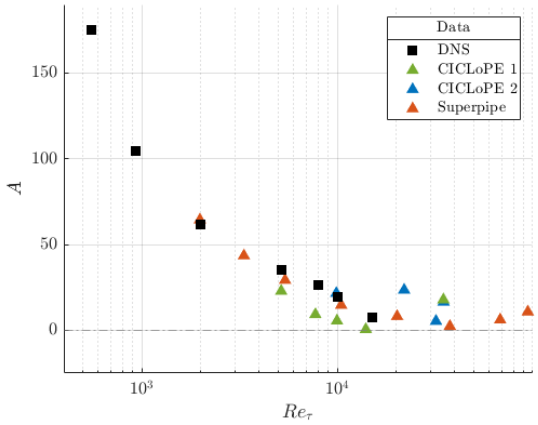

Figure 6: Values for constant $A = a_{x_2}/a_{Sx}$ from eq. (16) fitted for $Re_\tau = 180 \ldots 9.4 \cdot 10^4$

practical importance for turbulence models, especially if statistical symmetries are included as for example in Klingenberg *et al.* (2020).

Summarizing, in this work we have extended the ideas from the works of Oberlack *et al.* (2022) and Hoyas *et al.* (2022) to higher moments from U_2 and U_3. Compared to the considerations in these two works, the instantaneous moments in the current work are not affected by the mean flow in x_1-direction and are therefore identical with the fluctuating moments in the respective direction. For these moments, we have shown that scaling laws derived from first principle symmetry theory and based on the underlying set of Navier-Stokes and statistical equations are valid and therefore hold even for fluctuating moments with much smaller absolute values and much more sensitive behavior than the moments in mean flow direction.

SG and MO acknowledge funding by the Deutsche Forschungsgemeinschaft (DFG, German Research Foundation) - SPP 2410 Hyperbolic Balance Laws in Fluid Mechanics: Complexity, Scales, Randomness (CoScaRa), within the Project "Approximation Methods for Statistical Conservation Laws of Hyperbolically Dominated Flow" under project number 526024901. SH is partially funded by project PID2021-128676OB-I00 by Ministerio de Ciencia, innovación y Universidades / FEDER.

REFERENCES

Görtz, S. & Oberlack, M. 2024 High-moment scaling laws of wall-bounded turbulent shear flows: Invariant solutions to the multi-point moment equations. *under review with Phys. Rev. Fluids* .

Hoyas, S. & Jiménez, J. 2006 Scaling of the velocity fluctuations in turbulent channels up to $Re_\tau = 2003$. *Phys. Fluids* **18** (1), 011702.

Hoyas, S., Oberlack, M., Alcántara-Ávila, F., Kraheberger, S. V. & Laux, J. 2022 Wall turbulence at high friction reynolds numbers. *Phys. Rev. Fluids* **7**, 014602.

Hultmark, M., Vallikivi, M., Bailey, S. C. C. & Smits, A. J. 2012 Turbulent pipe flow at extreme reynolds numbers. *Phys. Rev. Lett.* **108**, 094501.

Klingenberg, D., Plümacher, D. & Oberlack, M. 2020 Symmetries and turbulence modeling. *Phys. Fluids* **32**, 025108.

Lee, M. & Moser, R. D. 2015 Direct numerical simulation of turbulent channel flow up to $Re_\tau \approx 5200$. *J. Fluid Mech.* **774**, 395–415.

Oberlack, M. 2001 A unified approach for symmetries in plane parallel turbulent shear flows. *J. Fluid Mech.* **427**, 299–328.

Oberlack, M., Hoyas, S., Kraheberger, S. V., Alcántara-Ávila, F. & Laux, J. 2022 Turbulence statistics of arbitrary moments of wall-bounded shear flows: A symmetry approach. *Phys. Rev. Lett.* **128**, 024502.

Oberlack, M. & Peters, N. 1993 *Closure of the Two-Point Correlation Equation in Physical Space as a Basis for Reynolds Stress Models*, pp. 85–94. Elsevier Science.

Oberlack, M. & Rosteck, A. 2010 New statistical symmetries of the multi-point equations and its importance for turbulent scaling laws. *Discrete Continuous Dyn. Syst* **3**, 451–471.

Oberlack, M., Wacławczyk, M., Rosteck, A. & Avsarkisov, V. 2015 Symmetries and their importance for statistical turbulence theory. *Mechanical Engineering Reviews* **2** (2), 15–00157.

Rosteck, Andreas M. 2014 Scaling laws in turbulence - a theoretical approach using lie-point symmetries. PhD thesis, Technische Universität, Darmstadt.

Wacławczyk, M., Staffolani, N., Oberlack, M., Rosteck, A., Wilczek, M. & Friedrich, R. 2014 Statistical symmetries of the lundgren-monin-novikov hierarchy. *Physical Review E* **90** (1), 013022.

Yamamoto, Y. & Tsuji, Y. 2018 Numerical evidence of logarithmic regions in channel flow at $Re_\tau = 8000$. *Phys. Rev. Fluids* **3**, 012602.

Zimmerman, S., Philip, J., Monty, J., Talamelli, A., Marusic, I., Ganapathisubramani, B., Hearst, R. J., Bellani, G., Baidya, R., Samie, M. & et al. 2019 A comparative study of the velocity and vorticity structure in pipes and boundary layers at friction reynolds numbers up to 10^4. *J. Fluid Mech.* **869**, 182–213.

Örlü, R., Fiorini, T., Segalini, A., Bellani, G., Talamelli, A. & Alfredsson, P. H. 2017 Reynolds stress scaling in pipe flow turbulence—first results from ciclope. *Philosophical Transactions of the Royal Society A: Mathematical, Physical and Engineering Sciences* **375** (2089), 20160187.